Hindawi
Shock and Vibration
Volume 2023, Article ID 8561647, 15 pages
https://doi.org/10.1155/2023/8561647

Research Article

Dynamic Response of Curved Tunnels under Vertical Incidence of Transversal SV Waves

Huiling Zhao,[1] **Yuheng Ma**,[2] **and Xupeng Yao**[2]

[1]*College of Civil Engineering, Tongji University, Shanghai 200092, China*
[2]*School of Mechanics and Engineering Science, Shanghai University, Shanghai 200444, China*

Correspondence should be addressed to Huiling Zhao; hlzhao@shu.edu.cn and Yuheng Ma; 2499626041@qq.com

Received 31 March 2022; Revised 22 June 2022; Accepted 23 July 2022; Published 25 April 2023

Academic Editor: Xiaochen Wei

Long tunnels often have curved sections when alignment designs are influenced by topography, adverse geology, and environmental factors. When the transversal SV wave is incident vertically, the curved section of the tunnel is subject to a connection between longitudinal and transversal loads, which are asymmetrical about the tunnel longitudinal axis. Compared to straight tunnels, curved tunnels are more complex in terms of forces and deformations and may become a key control section limiting the seismic safety of curved tunnels. To investigate the seismic response of curved tunnels, numerical simulations of curved tunnels with different radii of curvature under transversal SV seismic waves were carried out in this study. Local artificial boundaries were programmed and used for the 3D rock tunnel interaction system model to simulate semi-infinite rock and to eliminate fake reflections of seismic waves on local boundaries. The results show that longitudinal deformation and cross-sectional deformation occurred simultaneously in curved tunnels when the transversal SV wave was incident vertically. As the curvature increased, the longitudinal deformation of the curved tunnel increased. The cross-section of the tunnel was in oblique compression, and the cross-sectional internal force showed significant asymmetry. When the radius of curvature was 250 m, the difference in bending moment between the left and right haunch was 35.2%. These characteristics differ from those of straight tunnels and should be paid attention in the seismic design of curved tunnels.

1. Introduction

Underground structures such as tunnels are constrained by the surrounding soil or rock. During earthquakes, underground structures did not exhibit their own vibration characteristics compared with aboveground structures. It has been found that underground structures are more resistant to earthquakes [1–3]. However, since the 1970s, various degrees of damage to tunnels and metro stations in earthquakes have been reported extensively [4, 5]. The 1995 Hanshin earthquake in Japan caused the collapse of Daikai Station and severe damage to tunnels [6, 7]. The 2008 Wenchuan earthquake led to severe damage to several highway tunnels [8]. Therefore, in recent years, researchers have paid great attention to the seismic resistance of underground structures.

In general, SV seismic waves propagating perpendicular to the tunnel longitudinal axis cause circumferential deformation (elliptical shape), while propagation parallel to the tunnel longitudinal axis and oblique to the tunnel axis causes longitudinal tensile deformation and bending deformation. As tunnel construction is constrained by topography and other factors, long tunnels have curved alignment inevitably [9–11]. Take the underground metro network in Beijing as an example, the curved section accounted for nearly 30% of the total underground mileage in 2012 [12]. The tunnel moves horizontally when the transverse SV wave is incident vertically. The change in alignment leads to additional longitudinal effects on the curved tunnel, and these effects are asymmetrical about the tunnel longitudinal axis. Thus, the forces and deformations are more complex. The seismic response characteristics of curved tunnels need to be studied.

There have been some studies on the seismic response of curved structures. Lee and Hsiao [13] carried out a simplified in-plane free vibration analysis on curved nonuniform beams by introducing two physical parameters, which are the forces per unit arc length in the radial and tangential directions, respectively, caused by the radial displacement, and reached a solution for the free vibrations of curved beams with a constant radius. Li and Ren [14] employed the Galerkin method to obtain closed-form solutions for vertical, torsional, radial, and axial responses of a curved beam subjected to multidirectional moving loads. Yu et al. [15] considered the dynamic interaction between the tunnel and the foundation and proposed a new analytical solution for the dynamic response of curved tunnels based on small deformation analysis. Ma et al. [16] presented a curved two-and-a-half dimensional model and simulated the dynamic responses of the curved tunnel under earthquakes. The two-and-a-half dimensional model only can be used for analyzing the internal forces and deformations in the cross-section rather than the dynamic response along the longitudinal axis. In order to obtain a more realistic seismic response to the curved tunnel, it is necessary to establish a three-dimensional numerical model to simulate the complex soil structure interactions. Numerical models of curved tunnels with different radii of curvature were established to analyze the deformation and internal forces of curved tunnels when the transverse SV wave is incident vertically.

2. Partial Artificial Boundaries

The numerical model requires local site analysis around the tunnel to be intercepted from an infinite site, involving truncated boundaries and seismic wave input at the boundary. When the bedrock is very deep, an elastic foundation model is required to account for the dissipation of seismic waves deep into the ground. The widely used seismic wave input methods for elastic foundation models are viscous [17] or viscoelastic [18] boundaries and the corresponding equivalent nodal load inputs. Viscous and viscoelastic boundaries are used to dissipate outgoing waves from inside the model to infinity and to avoid boundary reflections. Joyner et al. [19] gave equations for the equivalent nodal loads corresponding to the two boundaries and completed the time history inputs at the truncated boundary. Nielsen [20]and Zienkiewicz et al. [21] used free field boundaries to achieve automatic application of lateral equivalent nodal forces. In this study, the viscous boundary at the bottom and the free field boundary were used as local artificial boundaries, and then, the equivalent seismic load input was completed at the bottom in stress time history. The following is a simple example to verify the effectiveness of the local artificial boundary.

A 3D model with dimensions of $20\,m \times 10\,m \times 10\,\mathrm{m}$ was considered, and the grid size was 1 m. The top boundary was set as free, and the bottom and the 4 sides were applied as free field boundary conditions. The material properties for the site were set as that the modulus of elasticity was 24 MPa, density was 1000 kg/m^3, and Poisson's ratio was 0.2, which defined a shear wave speed of 100 m/s and a compressional wave speed of 163.3 m/s for the site. The pulse wave was input horizontally from the bottom of the model and propagated upwards. The expression for the pulse wave was

$$u(t) = \frac{1}{2}\left[1 - \cos\left(2\pi f t\right)\right], \quad (f = 4.0, 0 \le t \le 0.25s). \tag{1}$$

According to the one-dimensional wave theory, the horizontal shear wave reached the middle of the model at $t = 0.05$ s (5/100 = 0.05) and reached the top of the model at $t = 0.1$ s (10/100 = 0.1). The amplification factor was two because the top is a free surface. The ground shaking lasted for 0.25 s, so propagation ended at the top at $t = 0.35$ s. Seismic waves propagated downward after reflection from the top free surface, and at $t = 0.15$ s, it returned to the middle of the model and was superimposed on the input wave. The propagation ended in the middle at $t = 0.4$ s. At $t = 0.2$ s, the reflected wave returned to the bottom of the model and was superimposed on the input wave, so propagation ended at the bottom at $t = 0.45$ s.

Velocity time history at different locations by theoretical analysis and numerical results from the model with local artificial boundary is compared in Figure 1. It can be seen that the two results match well.

Furthermore, soil tunneling interactions were considered and the ground displacement timescales corresponding to different burial depths were compared with the free field response to verify the reliability of the simulation in the presence of tunneling structures, as shown in Figure 2. The response of the soil tunnel model at the depth of the site is basically consistent with the free field model, with few differences in the near-surface soil response. In the soil tunnel model, as the seismic wave passes through the tunnel, the tunnel structure acts as entrainment in the seismic wave propagation path, causing scattering and wave field changes, which in turn affect the near-surface soil. The near-surface displacement response is slightly reduced relative to the free field, reflecting the effect of the presence of the tunnel structure on the seismic response of the site.

3. Numerical Modelling of Curved Tunnels

3.1. Tunnel Parameters. The cross-section of the mountain tunnel was formed by connecting four arcs with radii of 11.5 m, 5 m, 2.5 m, and 2.5 m, respectively. The buried depth of the tunnel was set at 10 m, and the lining thickness was 0.35 m. The Mohr–Coulomb model combining Rayleigh damping was used for the surrounding rock, and the elastic model was used for the lining. The model material parameters are given in Table 1. The research in this study only considered the dynamic response of the tunnel and surrounding rock under normal service conditions, and therefore, the effect of initial stress conditions and stress conditions during the construction of the tunnel was neglected in the model. The dynamic response of an earthquake refers to the incremental stress due to the seismic action.

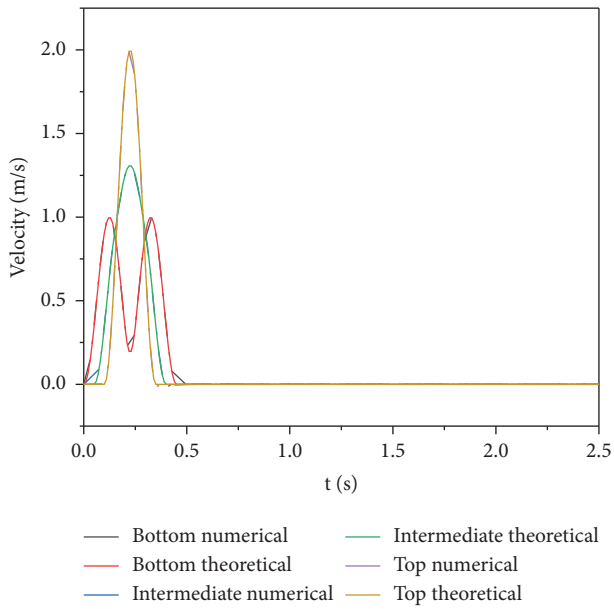

Figure 1: Velocity time history at different locations in theoretical and numerical results.

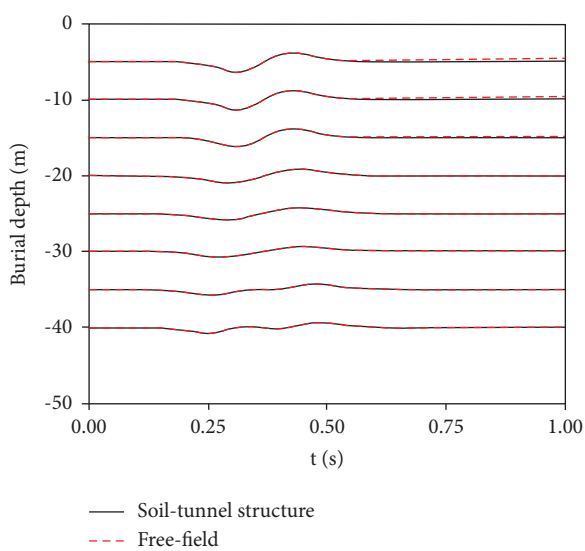

Figure 2: Comparison of the soil tunnel model with the free field model for horizontal displacement (magnification: 20 times).

3.2. 3D Numerical Model. A 3D model of the curved tunnel was created. The horizontal (x-direction) length was taken as 200 m, the longitudinal (y-direction) length as 250 m, and the vertical (z-direction) length as 40 m. Along the longitudinal direction, a section of tunnel with a straight-line alignment of 50 m length is first, connecting a curved tunnel section of 150 m length, and a section of tunnel with a straight-line alignment of 50 m length at last. As shown in Figure 3, for a curved tunnel, part of the tunnel was perpendicular to the vibration direction, part intersected the curve in the vibration direction, and part was oblique to the vibration direction. The viscous boundary at the bottom and the free field boundary at the side were set. The distance from the left and right and the bottom sides to the center of the tunnel was greater than three times the tunnel diameter. The vault, left and right spandrel, left and right haunches, left and right arch foots, and the arch bottom were taken as key monitoring points for each cross-section during the tunnel analysis.

3.3. Seismic Wave. The analysis focuses on the characteristics of the seismic response of curved tunnels and gaining a regular understanding to better guide engineering practice. The Ricker wavelet [22] has a wide frequency spectrum and a clear analytical formula, which can excite a sufficient response from the site and tunnel structure. Also, the Ricker wavelet time history curve has only one pulse waveform, which can provide concise simulation results and reveal the response characteristics of the site and tunnel structure. It has been widely adopted in the numerical simulation of the dynamic response of underground structures [23, 24], and the time history of the Ricker wavelet is defined as follows:

$$\alpha(t) = \left(1 - 2\pi^2 f_c^2 t^2\right)\exp\left(-\pi^2 f_c^2 t^2\right), \tag{2}$$

where f_c is the Ricker wavelet center frequency. The equivalent shear wave velocity of soil given in Table 1 is 610 m/s and the thickness of soil is 40 m. The seismic period of soil can be calculated according to the theoretical formula [25] as 0.26 s, which is about 4 Hz. Figure 4 shows the time curve and spectrum of the Ricker wavelet with a velocity amplitude of 1 m/s and a center frequency of 4 Hz.

4. Dynamic Response of Curved Tunnels

3D models of curved tunnels with different radii of curvature $r = 250$ m, $r = 350$ m, $r = 450$ m, and linear tunnels ($r = \infty$m) respectively, as shown in Figure 5 were established.

Figure 6 shows the velocity time history of the cross-sectional vault at $y = 125$ m for different radii of curvature. As the radius of curvature decreased, the amplitude of the x-direction velocity time history remained almost constant and the amplitude of the y-direction velocity time history increased. The y-direction velocity time history of the straight tunnel is zero. In the horizontal direction, the linear tunnel only vibrated in the x-direction but not in the y-direction, while the curved tunnel vibrated in both the x and y directions.

4.1. Tunnel Axial Deformation. Figure 7 shows the total displacement of the vault for different radii of curvature at the moment of the maximum acceleration. The total displacement amplitude in the straight tunnel was large and the vault displacements remained consistent points. As the curvature increased, the total displacement amplitude of the curved tunnel decreased and the displacement amplitude changed significantly along the longitudinal axis. Displacement differences can lead to large internal forces and deformations within curved tunnels, which exhibited different dynamic response characteristics compared with straight tunnels.

Table 1: Parameters of rock and tunnel materials.

Material	Density (kg/m^3)	Young's modulus/GPa	Poisson's ratio	Cohesion/MPa	Friction angle (°)
Tunnel	2500	34.5	0.2		
Surrounding rock	1900	1.8	0.4	0.05	23

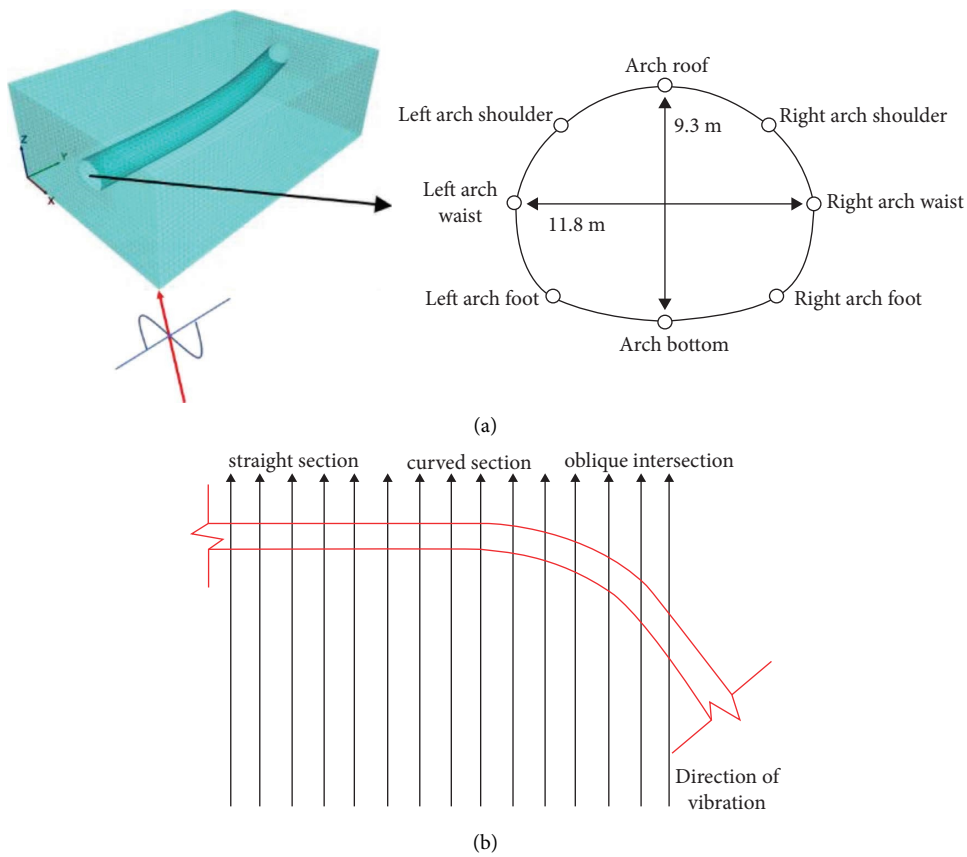

Figure 3: Schematic diagram of seismic action in a curved tunnel: (a) 3D view and cross-section. (b) 2D view.

The displacement time history of the vault at each key cross-section was monitored along the tunnel's longitudinal axial direction. These important cross-sections were located in the straight section ($y = 30$ m), at the connection of straight and curved ($y = 50$ m), in the middle of the curved section ($y = 125$ m), and at the end of the curved section ($y = 180$ m). The time history of the x and y-direction displacements at each monitoring point is shown in Figure 8. As shown in Figure 8(a), the closer the section of the curve, the smaller the peak displacement in the x-direction. At $t = 0.45$ s, the x-direction displacement of the straight section was 1.17 mm and that of the connection between the straight and curved was 1.14 mm, a decrease of 2.56% compared to the straight section. The x-direction displacement in the middle of the curve was 1.02 mm, a decrease of 12.8% compared to the straight section. The x-direction displacement at the end of the curve section was 0.96 mm, a decrease of 17.9% compared to the straight section. In summary, in terms of x-direction displacement, the introduction of a curved section resulted in a slight reduction in the peak displacement in that direction. Figure 8(b) shows the y-direction displacement time history of each section. The y-direction displacement amplitude of each section was significantly smaller than the x-direction. At $t = 0.5$ s, the y-direction displacement at the end of the curve section was 0.21 mm, while the x-direction displacement at the same time was 1.12 mm. The y-direction displacement was 18.75% of the x-direction displacement, indicating that the introduction of the curve section will result in a y-direction time history, but the tunnel dynamic response was still dominated by the x-direction. The y-direction displacements of each critical section differed in amplitude and can have opposite direction components. At the moment $t = 0.5$ s, the y-direction displacement at the end of the curved section was 0.156 mm, while the y-direction displacement of the straight section was −0.138 mm, indicating a tensile deformation of the curved tunnel along the tunnel axis.

The time history of the displacement of the vault in the cross-section along the axis of the straight tunnel is shown in Figure 9. The peak x and y-direction displacements along the axis of the straight tunnel were symmetrically distributed about the middle cross-section. Compared to the curved

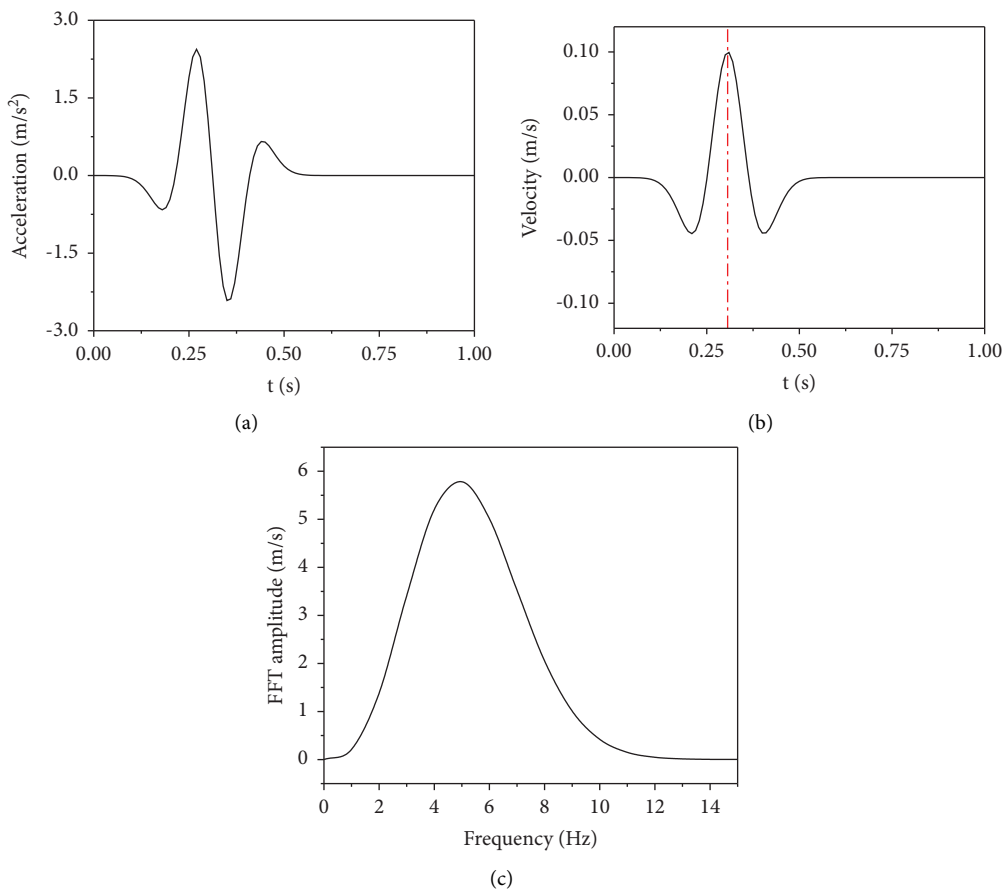

Figure 4: Input ground motion. (a) Acceleration time history. (b) Velocity time history. (c) Frequency spectrum.

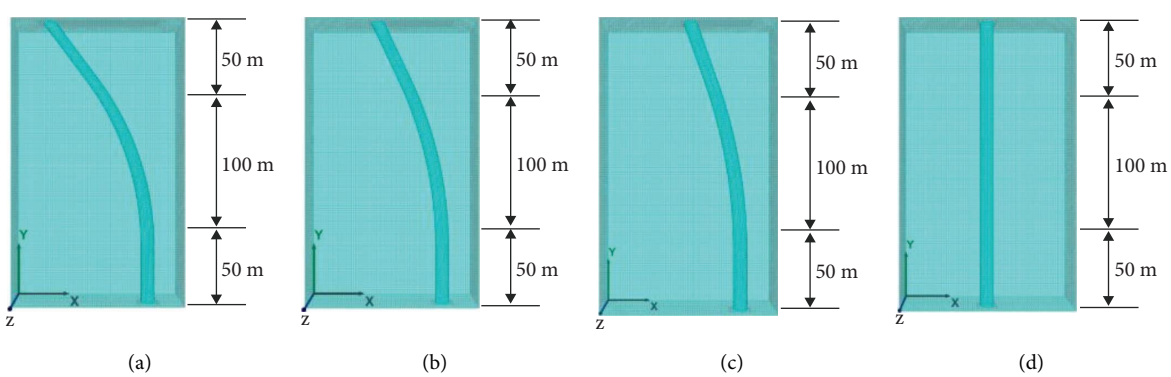

Figure 5: Tunnel numerical models with different curvature radii. (a) $r = 250$ m. (b) $r = 350$ m. (c) $r = 450$ m. (d) $r = \infty$.

tunnel, the peak x-direction displacement in the middle cross-section of the straight tunnel was almost constant, while the peak y-direction displacement varies considerably: the peak y-direction displacement in the middle of the curved section of the curved tunnel was 0.16 mm, while in the straight tunnel, it was almost 0 mm. In summary, the curved section leads to y-direction displacement of the tunnel structure, which, although small, can be considered as an additional effect of the change in alignment of the curved tunnel.

As shown in Figure 10, the displacement time history of the middle cross-sectional vault is compared for different radii of curvature. The radius of curvature had little effect on the displacement time history in the x-direction, and the amplitudes were very close to $r = 250$ m, $r = 350$ m, $r = 450$ m, and $r = \infty$ m. The radius of curvature has a significant effect on the Y-directional displacement time history. At $t = 0.375$ s, the amplitude was 0.22 mm at a radius of curvature of 250 m, 0.16 mm at a radius of curvature of 350 m by a decrease of 27.3%, and 0.11 mm at a radius of curvature of

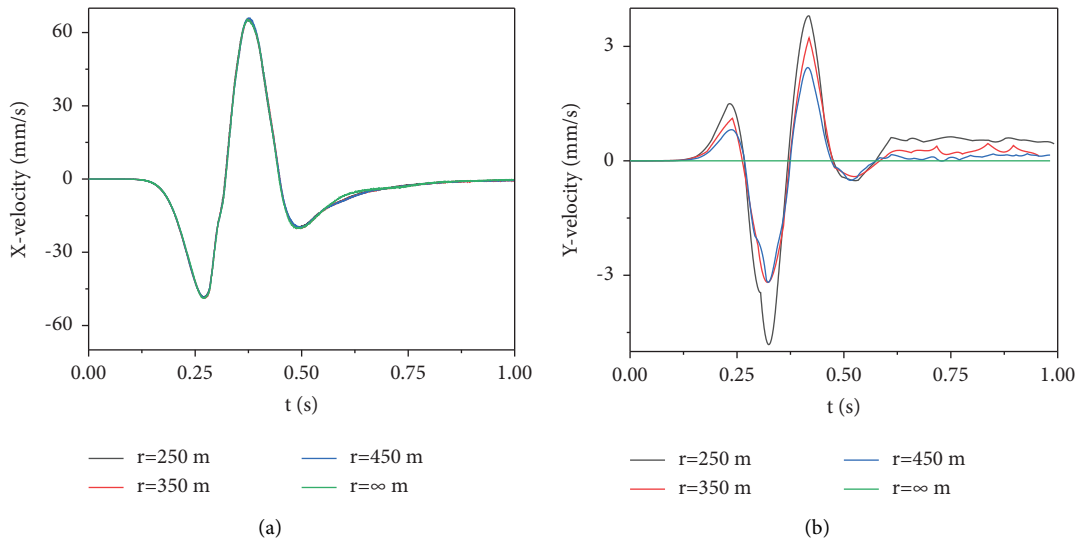

Figure 6: Velocity time history of the vault at (y) = 125 m of the curved tunnels with different curvature radii. (a) X-velocity time history. (b) Y-velocity time history.

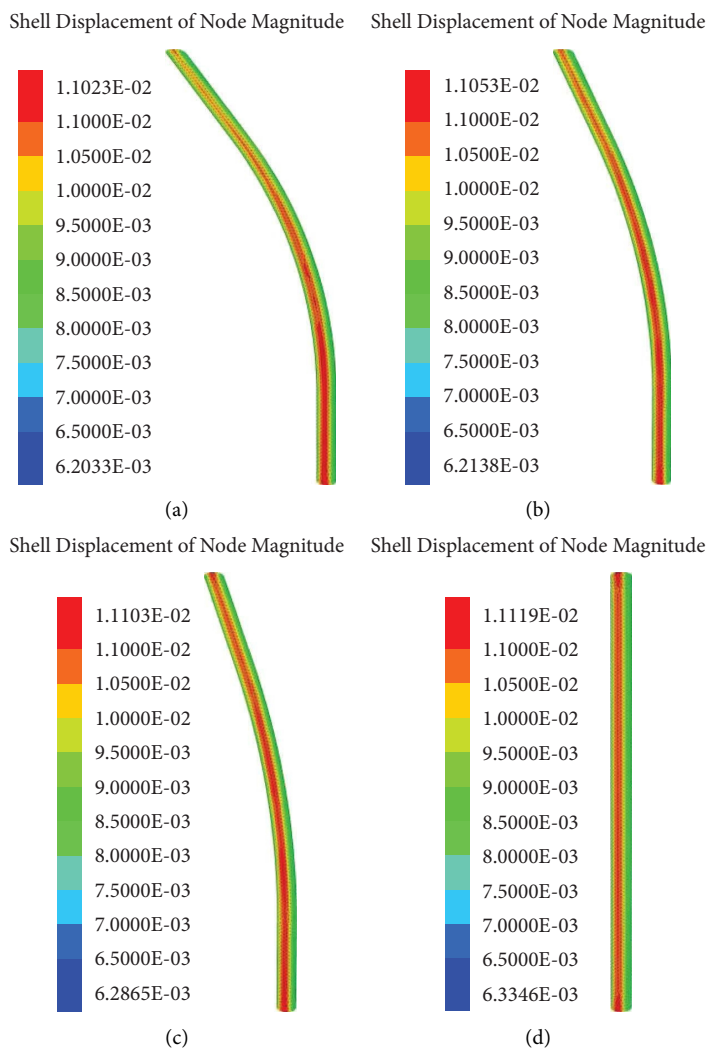

Figure 7: Total displacement contours of the curved tunnel with different curvature radii (unit: (m)): (a) $r = 250$ m. (b) $r = 350$ m. (c) $r = 450$ m. (d) $r = \infty$ m.

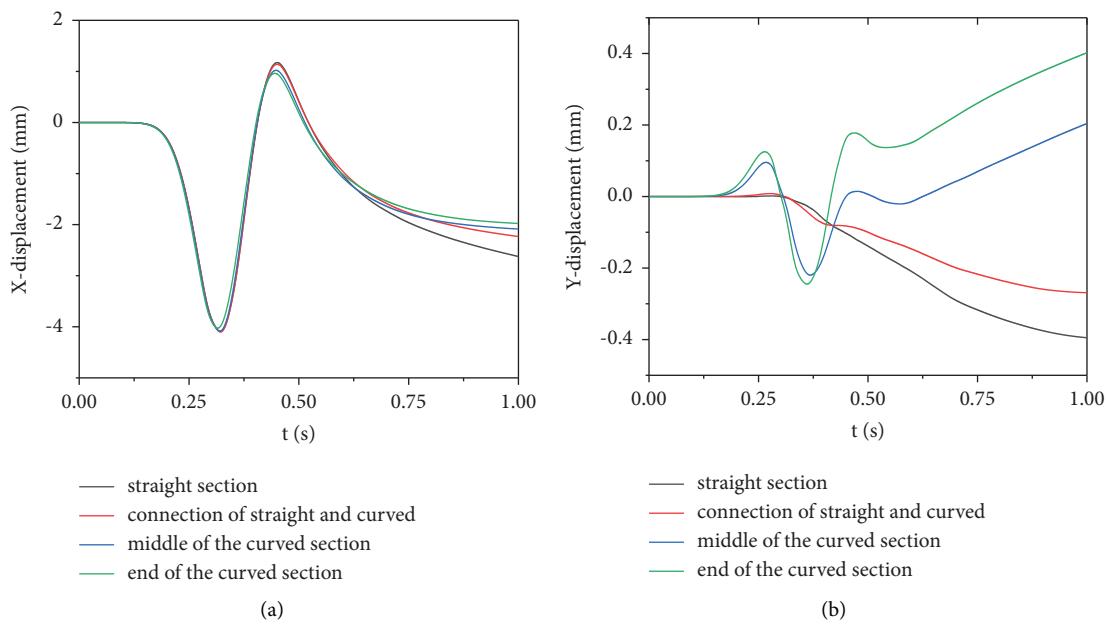

Figure 8: Displacement time history of the vault at key cross-sections of the curved tunnel. (a) Displacement in x-direction. (b) Displacement in y-direction.

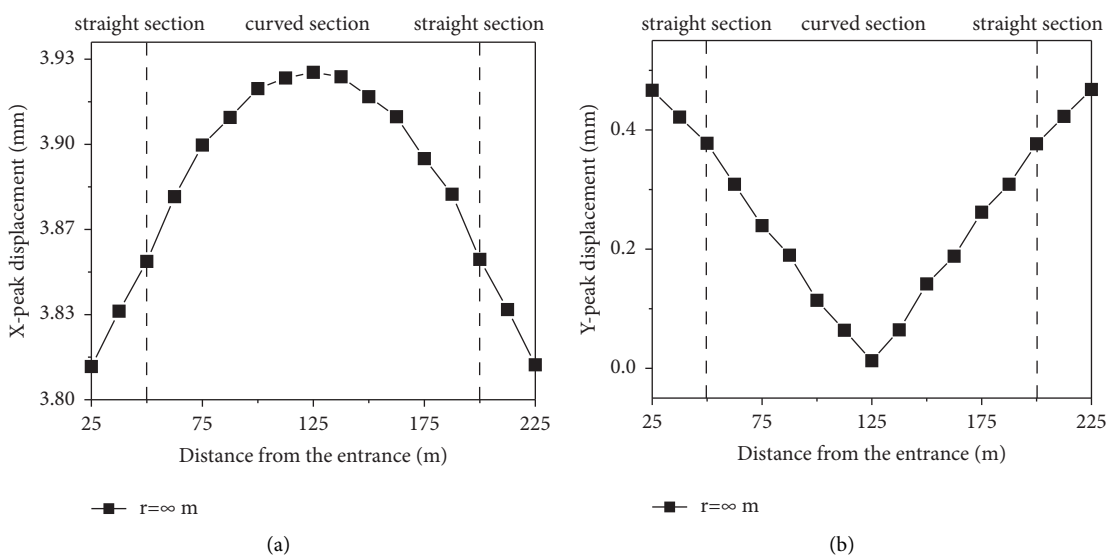

Figure 9: Peak displacement of the vault at different cross-sections along the straight tunnel. (a) Displacement in x-direction. (b) Displacement in y-direction.

450 m by a decrease of 50%. The effect of the radius of curvature on the displacement response of curved tunnels was therefore mainly reflected in the y-direction time history. The introduction of a curved section caused y-direction tensile deformation on the tunnel axis. Y-directional tensile deformation increased as the radius of curvature decreased.

Figure 11 shows a y-direction displacement contour along the tunnel axis. The y-direction displacements were not equal between the left and right sides of the curved tunnel, while the y-direction displacements on the left and right sides of the straight tunnel were basically the same, without relative displacements. In the case of the curved tunnel cross-section, y-direction displacements oppositely occur on its left and right sides, indicating that axial deformation has occurred and that the amount of axial deformation was not uniform along the axial direction.

Figure 12 shows the peak y-direction displacement of the vault along the axis for different radii of curvature. At the smallest radius of curvature ($r = 250$ m), the peak displacement occurred at the middle of the curve section ($y = 125$ m). As the radius of curvature increased, the peak displacement appeared progressively further back, and the peak displacement occurs at $y = 150$ m when $r = 350$ m and at $y = 225$ m when $r = 450$ m. The peak y-direction

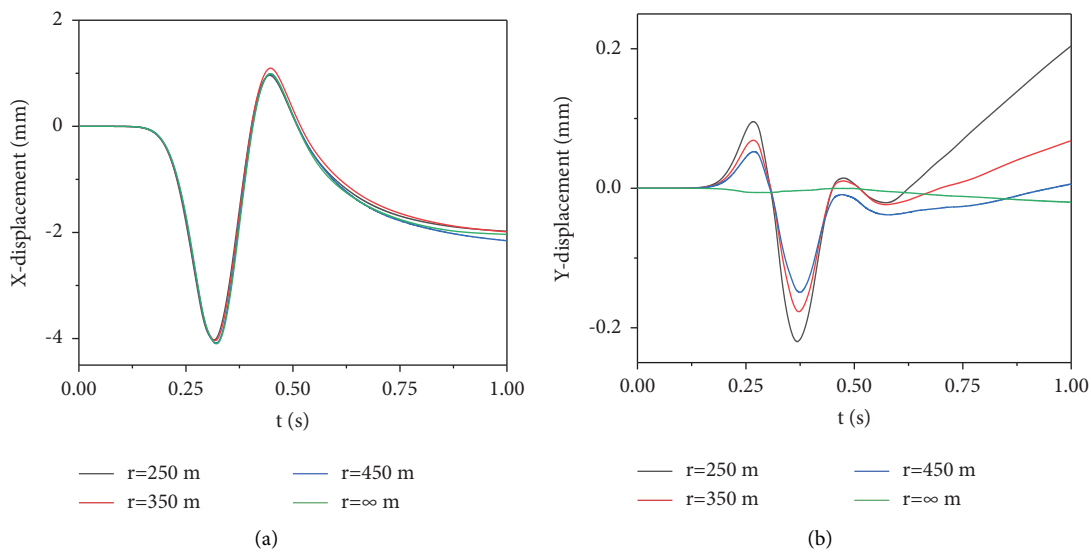

Figure 10: Displacement time history of the vault at $y = 125$ m cross-section of the curved tunnel with different curvature radii. (a) Displacement in x-direction. (b) Displacement in y-direction.

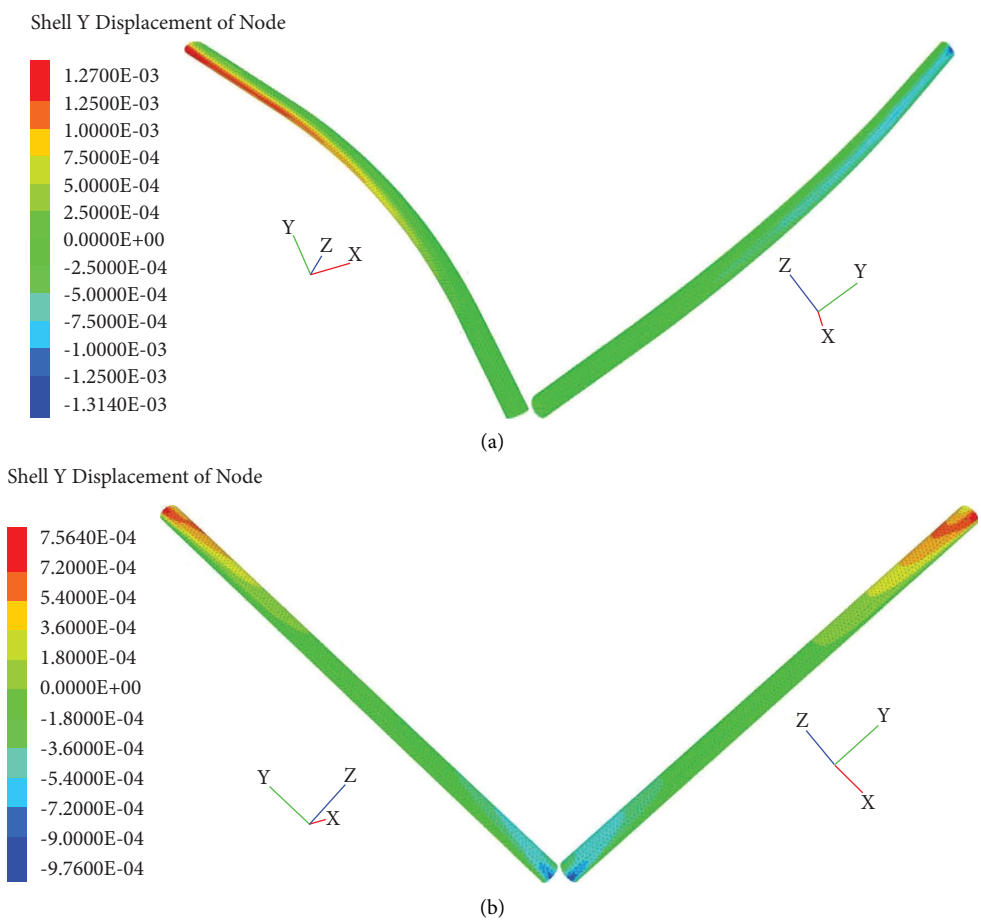

Figure 11: Y-directional displacement contour of the curved tunnel with different curvature radii (unit: (m)). (a) $r = 250$ m. (b) $r = \infty$ m.

displacements occurred at different locations for different radii of curvature, indicating that the alignment has a significant effect on the y-direction dynamic response.

Figure 13 shows the y-direction relative displacement of the left and right haunches at each key section for a radius of curvature of 250 m. The connection between straight and

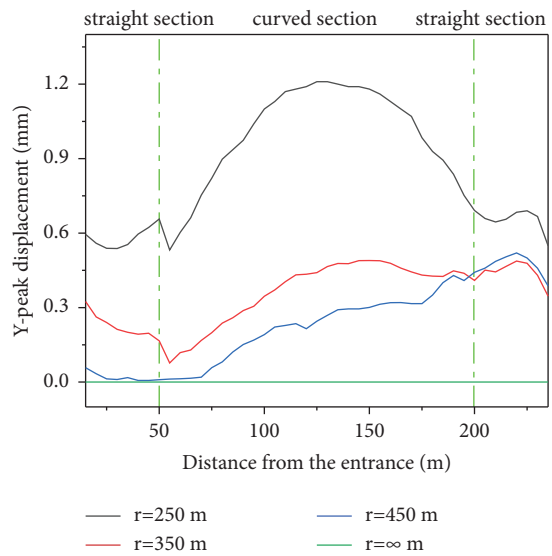

Figure 12: Peak displacement of the vault along the axis of the curved tunnel with different curvature radii.

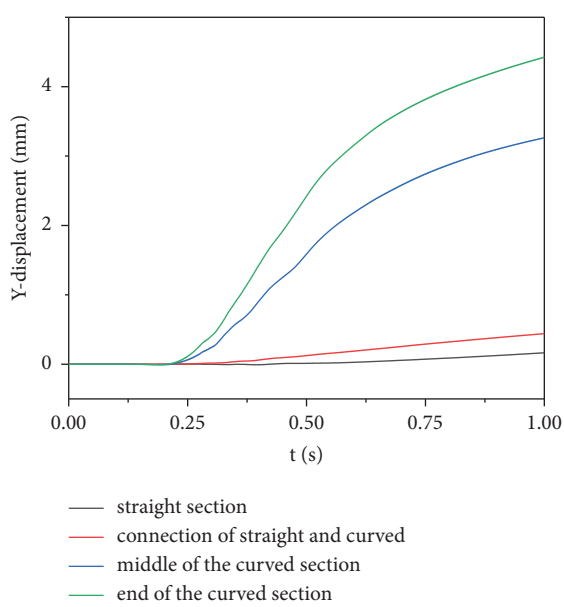

Figure 13: Y-directional relative displacement of the left and right haunches at key cross-sections of the curved tunnel.

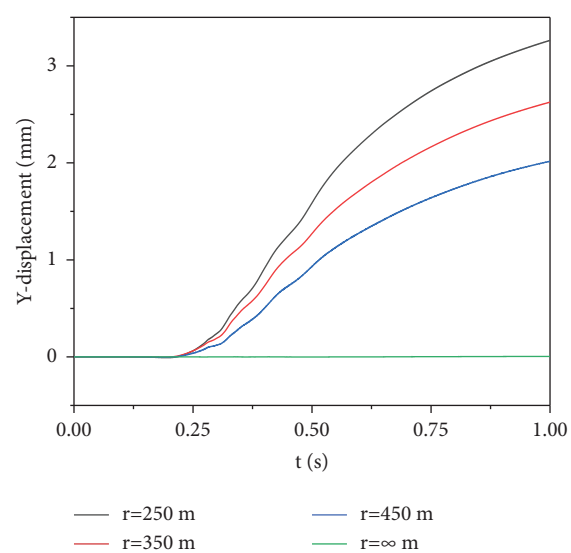

Figure 14: Y-directional relative displacement of the left and right haunches of the curved tunnel with different curvature radii.

curved was influenced by the introduction of the straight section. The axial deformation was only 0.2 mm, the axial deformation in the middle of the curve section was 3.1 mm, and the axial deformation at the end of the curve section was 4.4 mm. It was found that the closer to the end of the curved section, the more pronounced the axial deformation. Figure 14 shows the y-direction relative displacement of the left and right haunches for different radii of curvature. Y-directional relative displacement increased with the tunnel curvature. It can be seen that the curved tunnel undergoes significant axial deformation compared to the straight tunnel. The deformation becomes more pronounced as the curved section was approached and the curvature becomes greater.

4.2. Cross-Sectional Deformation. Figure 15 shows the x-direction displacement contour at some moment for the left and right sides of the curved and straight tunnels. As for the curved tunnel, the left and right in the x-direction were different, and the amount of relative displacement varied along the tunnel axis. As for the straight tunnel, the relative displacement was kept the same along the tunnel axis. Curved tunnels with inconsistent radial deformation of the cross-section along the axis may show a significant concentration of internal forces where the deformation changes abruptly.

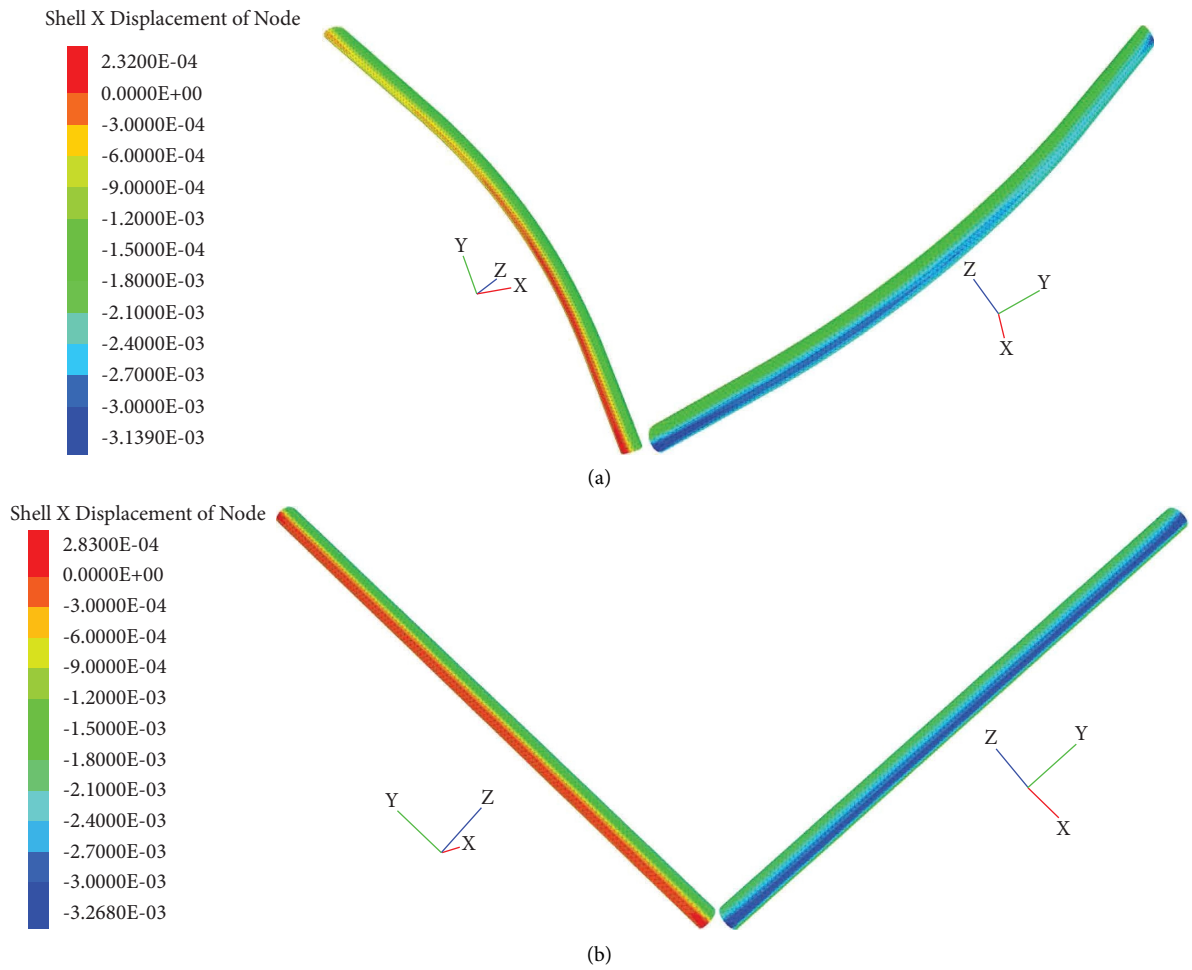

Figure 15: X-directional displacement contour of the curved tunnel with different curvature radii (unit: (m)). (a) $r = 250$ m. (b) $r = \infty$ m.

Figure 16 shows the z-direction displacement contour of the tunnel cross-section at the same moment, the z-direction displacement distribution varies for different radii of curvature. As the alignment curvature increased, the peak displacement was biased from the symmetry axis of the cross-section. Oblique compression was shown, resulting in the vertical inconsistent deformation of the cross-section. Figure 17 shows the relative horizontal x-directional displacement of the left and right haunch and the relative z-directional displacement of the vault and the arch bottom of the curved tunnel for different radii of curvature. As the radius of curvature decreased, both the peak relative displacements in the x-direction of the left and right haunch and the peak relative displacements in the z-direction decreased. The cross-sectional deformation was reduced in curved tunnels compared with straight tunnels.

Figure 18 shows the relative deformation of the left and right haunches at each critical section monitored when the radius of curvature was 250 m. The closer to the straight section, the greater the relative displacement in the x and z directions of the left and right haunches. The x and z-directional deformations in the straight section were 15.8 mm and 25 mm, respectively, while the x and z-directional deformations at the end of the curved section were 7.8 mm and 10.1 mm, respectively, a reduction of 50.6% and 59.6%. As with the transition between straight and curved sections, the connection between straight and curved was affected by the inconsistencies in the amount of deformation between the two and required significant attention.

4.3. Internal Forces in the Tunnel. For compression-bending elements, such as tunnel linings, the bending moment was the key variable controlling the design, and the weak points of the tunnel's seismic resistance can be determined according to the law of moment distribution. For the tunnel structure in this study, the y-directional bending moment diagram for the cross-sections is shown in Figure 19.

Figure 20 shows the y-directional bending moments on the left and right sides of the curved tunnel at the same moment for different radii of curvature. As the radius of curvature decreased, the bending moment distribution between the left and right sides showed more asymmetry. At $r = 250$ m, asymmetrical forces appeared from the connection of straight and curved to the end of the tunnel. It shows a similar pattern to the location of the peak y-direction displacement, where the peak bending moment in the curved section indicated a significant stress concentration.

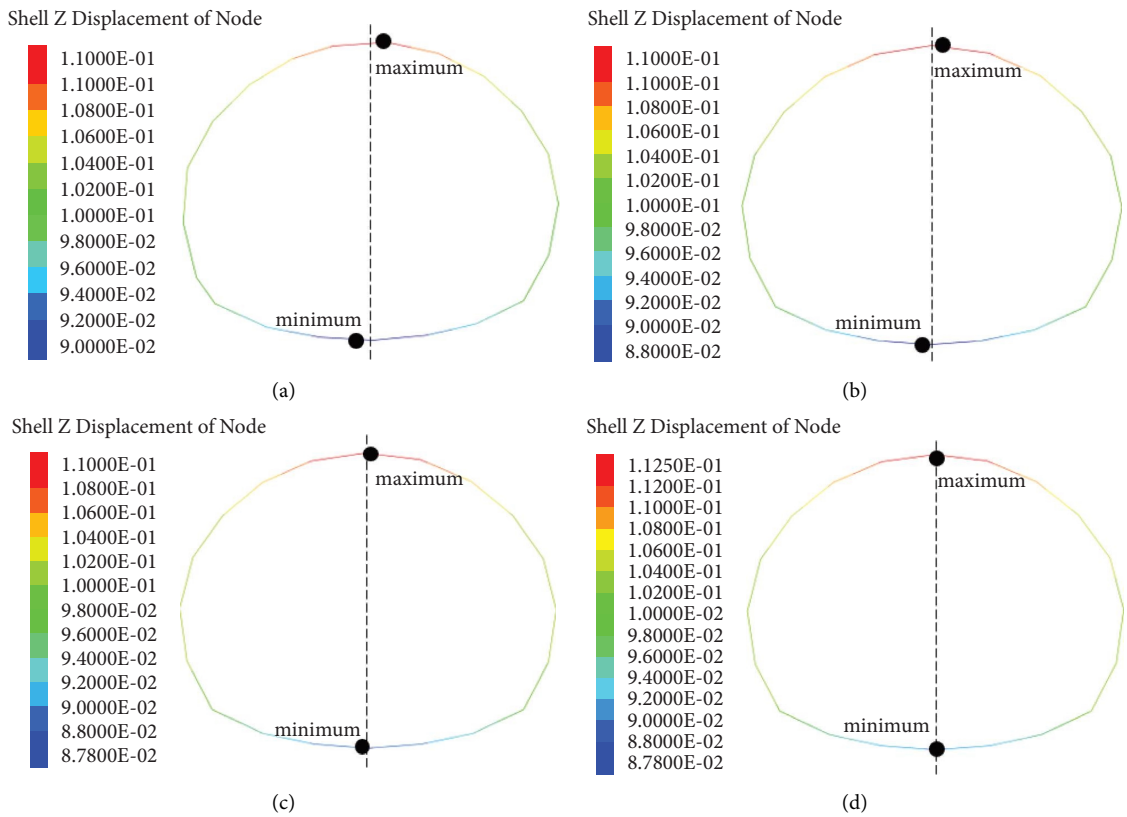

Figure 16: Z-directional displacement contour of the curved tunnel with different curvature radii (unit: (m)): (a) $r = 250$ m. (b) $r = 350$ m. (c) $r = 450$ m. (d) $r = \infty$ m.

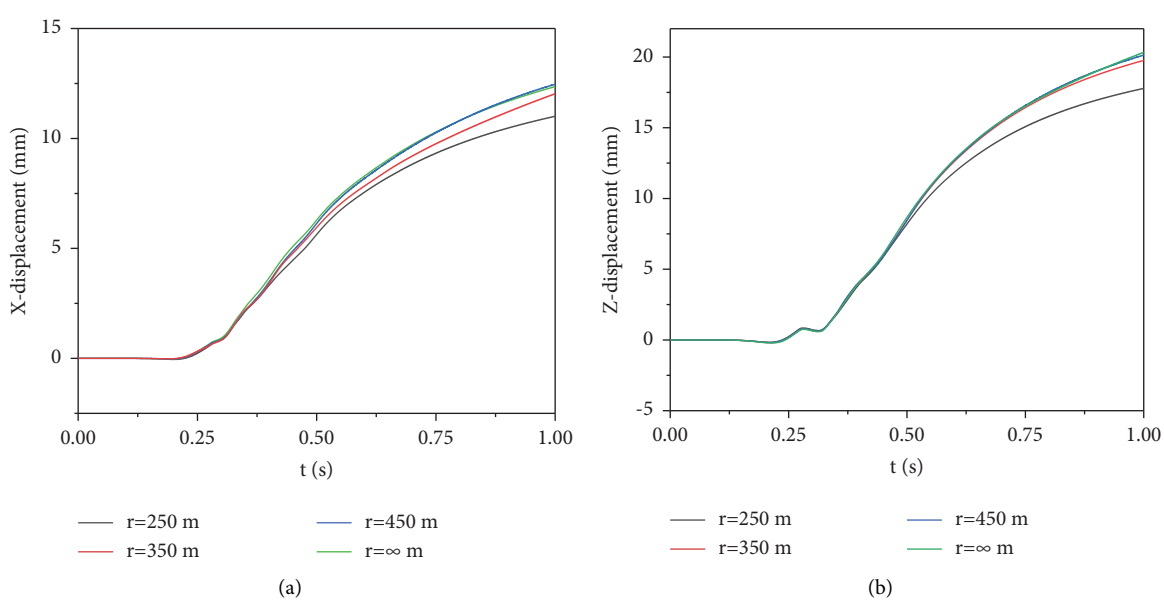

Figure 17: Relative displacement time history at $y = 125$ m cross-section of the curved tunnel with different curvature radii: (a) X-directional relative displacement of the left and right haunches. (b) Z-directional relative displacement of the vault and bottom.

The peak y-directional bending moments at each key position of the intermediate cross-section under different radii of curvature were compared and are given in Table 2. The radius of curvature changed the internal force distribution of the lining structure. At each radius of curvature, there was a pattern that the internal force on the left side of the cross-section (left arch spandrel, left haunch, and left arch foot) was greater than that on the

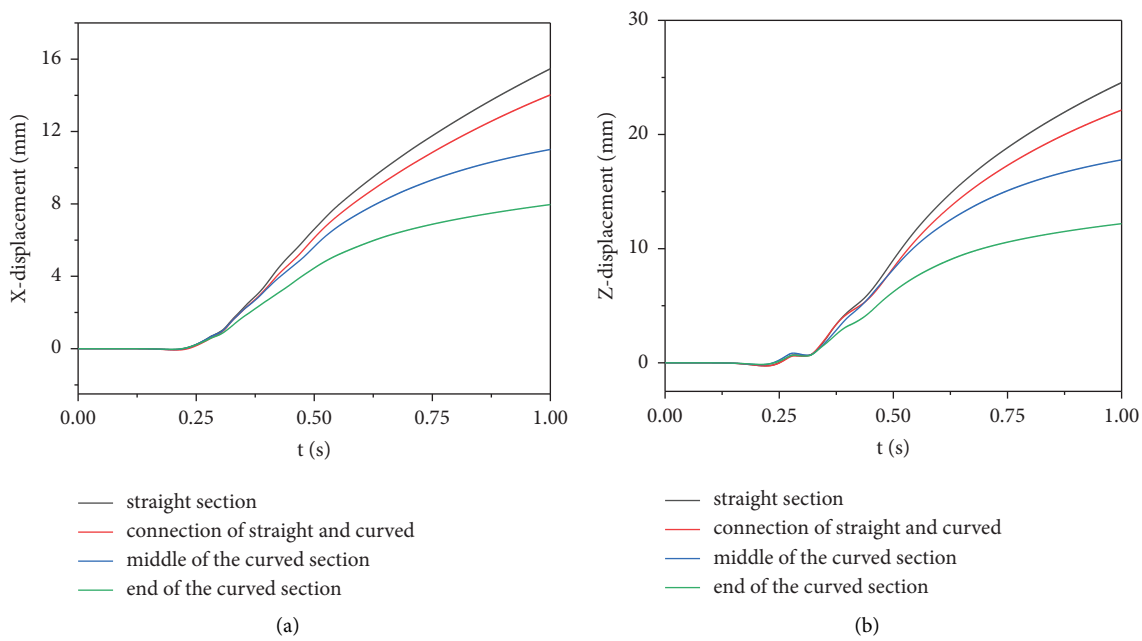

Figure 18: Relative displacement time history of the vault at key positions of the curved tunnel: (a) X-directional relative displacement of the left and right haunches. (b) Z-directional relative displacement of the vault and bottom.

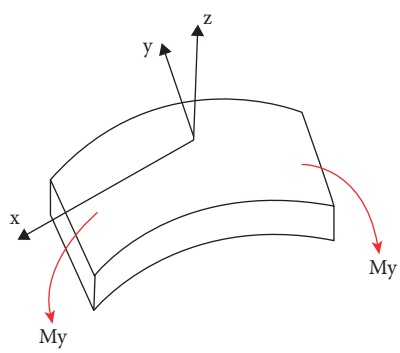

Figure 19: Direction of bending moment $(M)_y$ diagram.

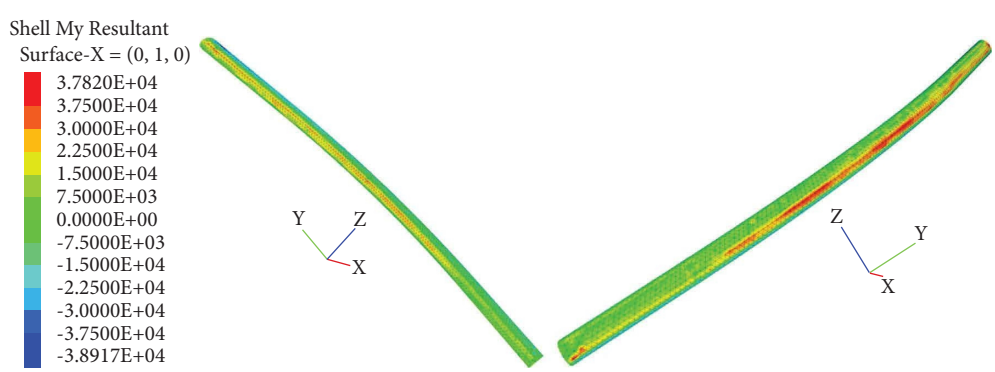

(a)

Figure 20: Continued.

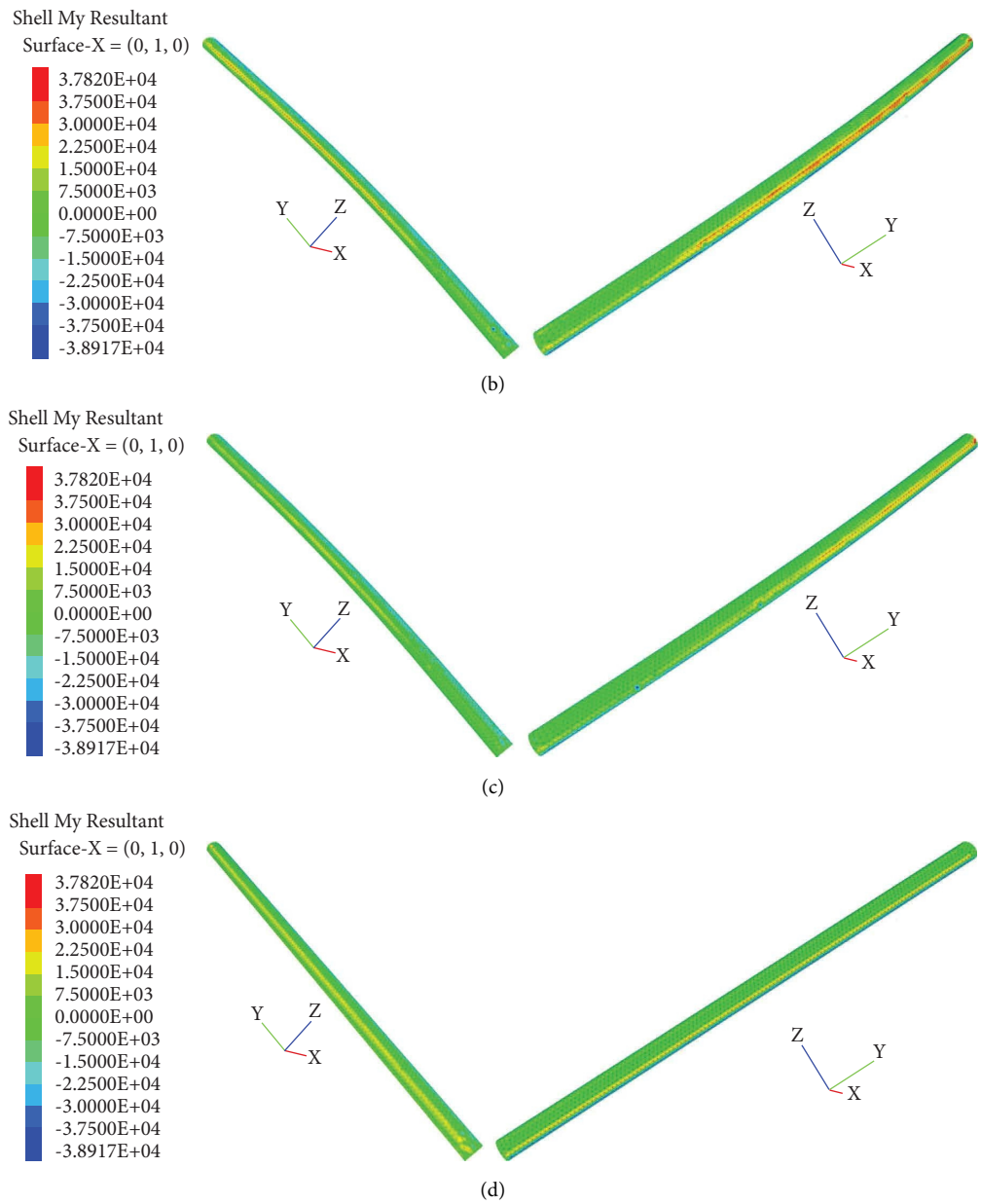

Figure 20: Y-directional bending moment contour of the curved tunnel with different curvature radii (unit: N·m). (a) $r = 250$ m. (b) $r = 350$ m. (c) $r = 450$ m. (d) $r = \infty$ m.

Table 2: Peak bending moment at tunnel monitoring points (unit: kN·m).

	$r = 250$ m	Difference in internal forces (%)	$r = 350$ m	Difference in internal forces (%)	$r = 450$ m	Difference in internal forces (%)
Vault	87.6		69.8		70.5	
Left arch spandrel	43.1		50.1		51.5	
Right arch spandrel	64.7	33.3	66.3	32.3	72.5	21
Left haunch	86.7	35.2	78.4	29.9	67.7	27.3
Right haunch	56.2		54.9		49.2	
Left arch foot	82.1	30.9	80.5	26.2	75.7	21.9
Right arch foot	56.7		59.4		59.1	
Arch bottom	74.0		83.6		65.4	

right side (right arch spandrel, right haunch, and right arch foot). The reason may be that the SV wave was incident on the left side of the model, and the curved tunnel also bended continuously to the left side of the model. At $r = 250$ m, $r = 350$ m, and $r = 450$ m radii of curvature, the asymmetric forces at the left and right arches of the intermediate cross-section were 35.2%, 28.3%, and 27.3%, respectively, and the asymmetric forces at $r = 250$ m increased by about 7.9% compared to those at $r = 450$ m. It was due to the fact that the smaller the radius of curvature, the more significantly the curved tunnel bended to the left side of the model, exacerbating the asymmetric forces on the left and right sides of the cross-section. In summary, the focus should be on the internal forces in the left haunch of the curved tunnel with a small radius of curvature under the transverse vertical incidence of the SV wave.

5. Conclusions

In this study, a three-dimensional numerical model was established to analyse and explore the dynamic response of curved tunnels when the transverse SV wave was incident vertically, and the main conclusions are summarized as follows.

(1) For a curved tunnel, part of the tunnel is perpendicular to the direction of vibration, part is intersected the curve in the direction of vibration, and part is oblique to the direction of vibration. Compared to linear tunnels, the curvature varying section of the tunnel is important for the safety control of the tunnel.

(2) The radial deformation in the cross-section of curved tunnel was slightly reduced compared to the straight tunnel. As the radius of curvature decreased, the oblique compression increased. Thus, attention needs to be paid to the location where the radial deformation changes abruptly, such as the connection between curved and straight.

(3) The deformation of curved tunnels along the axis was inconsistent, requiring a focus on the middle and end of the curved section. As the radius of curvature decreased, the axial deformation became complex.

(4) As the radius of curvature decreased, the asymmetrical forces on the left and right sides of the tunnel increased, and the internal forces on the tunnel structure became more damaging.

Data Availability

The data used to support the findings of this study are included within the article.

Acknowledgments

The authors acknowledge the financial support from the Shanghai Natural Science Foundation (19ZR1418700) and the National Natural Science Foundation of China (42277163).

Conflicts of Interest

The authors declare that they have no conflicts of interest.

References

[1] Y. M. A. Hashash, J. J. Hook, B. Schmidt, and J. I-Chiang Yao, "Seismic design and analysis of underground structures," *Tunnelling and Underground Space Technology*, vol. 16, no. 4, pp. 247–293, 2001.

[2] G. Tsinidis, F. De Silva, I. Anastasopoulos et al., "Seismic behaviour of tunnels: from experiments to analysis," *Tunnelling and Underground Space Technology*, vol. 99, Article ID 103334, 2020.

[3] K. Pitilakis and G. Tsinidis, "Performance and seismic design of underground structures[M]," *Earthquake Geotechnical Engineering Design*, pp. 279–340, Springer, Cham, 2014.

[4] T. Ariman and G. E. Muleski, "A review of the response of buried pipelines under seismic excitations," *Earthquake Engineering & Structural Dynamics*, vol. 9, no. 2, pp. 133–152, 1981.

[5] C. H. Dowding and A. Rozan, "Damage to rock tunnels from earthquake shaking," *Journal of the Geotechnical Engineering Division*, vol. 104, no. 2, pp. 175–191, 1978.

[6] H. Iida, T. Hiroto, N. Yoshida, and M. Iwafuji, "Damage to Daikai subway station," *Soils and Foundations*, vol. 36, no. Special, pp. 283–300, 1996.

[7] X. An, A. A. Shawky, and K. Maekawa, "The collapse mechanism of a subway station during the Great Hanshin earthquake," *Cement and Concrete Composites*, vol. 19, no. 3, pp. 241–257, 1997.

[8] H. Yu, J. Chen, A. Bobet, and Y. Yuan, "Damage observation and assessment of the Longxi tunnel during the Wenchuan earthquake," *Tunnelling and Underground Space Technology*, vol. 54, pp. 102–116, 2016.

[9] A. M. M. Wood, "The circular tunnel in elastic ground," *Géotechnique*, vol. 25, no. 1, pp. 115–127, 1975.

[10] G. Russo, C. Viggiani, and G. M. B. Viggiani, "Geotechnical design and construction issues for Lines 1 and 6 of the Naples Underground/Geotechnische Planung und Ausführung der U-Bahnlinien 1 und 6 in Neapel," *Geomechanics and Tunnelling*, vol. 5, no. 3, pp. 300–311, 2012.

[11] S. Fabozzi, E. Bilotta, H. Yu, and Y. Yuan, "Effects of the asynchronism of ground motion on the longitudinal behaviour of a circular tunnel," *Tunnelling and Underground Space Technology*, vol. 82, pp. 529–541, 2018.

[12] Y. Yuan, W. N. Liu, and W. F. Liu, "Propagation law of ground vibration in the curve section of metro based on in-situ measurement," *China Railway Science*, vol. 33, no. 4, pp. 133–138, 2012.

[13] S. Y. Lee and J. Y. Hsiao, "Free in-plane vibrations of curved nonuniform beams," *Acta Mechanica*, vol. 155, no. 3-4, pp. 173–189, 2002.

[14] S. H. Li and J. Y. Ren, "Analytical study on dynamic responses of a curved beam subjected to three-directional moving loads," *Applied Mathematical Modelling*, vol. 58, pp. 365–387, 2018.

[15] H. Yu, X. Li, and P. Li, "Analytical solution for vibrations of a curved tunnel on viscoelastic foundation excited by arbitrary dynamic loads," *Tunnelling and Underground Space Technology*, vol. 120, Article ID 104307, 2022.

[16] L. Ma, H. Ouyang, C. Sun, R. Zhao, and L Wang, "A curved 2.5D model for simulating dynamic responses of coupled track-tunnel-soil system in curved section due to moving

loads," *Journal of Sound and Vibration*, vol. 451, pp. 1–31, 2019.

[17] J. Lysmer and R. L. Kuhlemeyer, "Finite dynamic model for infinite media," *Journal of the Engineering Mechanics Division*, vol. 95, no. 4, pp. 859–877, 1969.

[18] A. J. Deeks and M. F. Randolph, "Axisymmetric time-domain transmitting boundaries," *Journal of Engineering Mechanics*, vol. 120, no. 1, pp. 25–42, 1994.

[19] W. B. Joyner and A. T. F. Chen, "Calculation of nonlinear ground response in earthquakes," *Bulletin of the Seismological Society of America*, vol. 65, no. 5, pp. 1315–1336, 1975.

[20] A. H. Nielsen, "Absorbing boundary conditions for seismic analysis in ABAQUS," in *Proceedings of the ABAQUS users' conference*, pp. 359–376, Beijing China, June 2006.

[21] O. C. Zienkiewicz, N. Bicanic, and F. Q. Shen, "Earthquake input definition and the trasmitting boundary conditions," *Advances in Computational Nonlinear Mechanics*, pp. 109–138, Springer, Vienna, 1989.

[22] N. Ricker, "The form and laws of propagation of seismic wavelets," *Geophysics*, vol. 18, no. 1, pp. 10–40, 1953.

[23] K. Pitilakis, G. Tsinidis, A. Leanza, and M. Maugeri, "Seismic behaviour of circular tunnels accounting for above ground structures interaction effects," *Soil Dynamics and Earthquake Engineering*, vol. 67, pp. 1–15, 2014.

[24] M. Panji and B. Ansari, "Transient SH-wave scattering by the lined tunnels embedded in an elastic half-plane," *Engineering Analysis with Boundary Elements*, vol. 84, pp. 220–230, 2017.

[25] E. F. Toro, "A weighted average flux method for hyperbolic conservation laws," *Proceedings of the Royal Society of London. A. Mathematical and Physical Sciences*, vol. 423, no. 1865, pp. 401–418, 1989.